Online-Journals.org

iJOE International Journal of Online and Biomedical Engineering

iJOE | eISSN: 2626-8493 | Vol. 20 No. 2 (2024) | OPEN ACCESS

https://doi.org/10.3991/ijoe.v20i02.44627

PAPER

The Impact of Using DPSK Modulation on the Performance of Transdermal Optical Wireless Communications under Pointing Errors

Yazeed Suleiman Al-Rbeihat(✉), Omar M. Hasan

Department of Communication Engineering, Princess Sumaya University for Technology, Amman, Jordan

yaz20208013@std.psut.edu.jo

ABSTRACT

The current paper explores the impact of misalignment between transceivers (referred to as pointing error (PE)) on the performance of transdermal optical wireless (TOW) technology, as indicated by average signal-to-noise ratio (SNR), outage probability (OP), outage rate (OR), and average ergodic capacity (AEC). This study was inspired by the effectiveness of differential phase shift keying (DPSK) in enhancing the reliability of the link in free-space optical communications (FSO). Furthermore, this enhancement was studied and analyzed in consideration of the impact of pointing errors. In particular, this paper presents a mathematical analysis that considers certain characteristics of the channel, limitations within the body, the pointing errors (PEs) between the transceivers, and other specific aspects of the optical unit. The results demonstrate the significant impact of PEs on the reliability of the TOW link and highlight the improvement provided by the DPSK technique. i.e., 3 dB better performance compared to the on-off keying (OOK) modulation technique. Finally, this research demonstrates the practical application of wireless optical technology in the medical field within the wavelength range of 800–1300 nm, with optimal performance observed around 1100 nm.

KEYWORDS

transdermal, differential phase shift keying (DPSK), average signal-to-noise ratio (SNR), outage probability (OP), outage rate (OR), average ergodic capacity (AEC), optics, transdermal optical wireless (TOW), optical wireless communication (OWC)

1 INTRODUCTION

Medical implants (MIs) and bio-devices have rapidly increased due to further research and studies on human diseases, as well as advancements in electronic circuits. One of these studies examines the use of wireless implantable sensors, which are inserted into the transdermal, also known as transcutaneous, using implant telemetry devices. It has recently been used for medical applications in the

Al-Rbeihat, Y.S., Hasan, O.M. (2024). The Impact of Using DPSK Modulation on the Performance of Transdermal Optical Wireless Communications under Pointing Errors. *International Journal of Online and Biomedical Engineering (iJOE)*, 20(2), pp. 131–148. https://doi.org/10.3991/ijoe.v20i02.44627

Article submitted 2023-09-01. Revision uploaded 2023-11-13. Final acceptance 2023-11-13.

human body [1]. According to the progression of the treatment, tailored to the illness, the patient's symptoms, and the case's condition, MIs are implanted for periods ranging from several months to many years, requiring higher data rates and lower power consumption [2]. The main categories of applications include cochlear implants, intraocular (retinal) implants, brain implant devices, pacemaker devices, and wireless capsule endoscopy. The increased availability of enhancements for a larger number of patients has sparked significant interest among academia and industries in MIs. Conventional MIs utilize the radio frequency (RF) band. They are known for being bandwidth (BW) saturated and typically have a transmission power estimated to be around tens of mW [3]. Transdermal communication could likely be achieved through RF wireless links. Nevertheless, while this type of innovation can deliver data rates of up to 24 Mbps, it also requires at least 30 mW [4], which results in significant power consumption for MIs, necessitating the replacement of RF with transdermal optical wireless (TOW). This paper sheds light on optical wireless communication (OWC) through transdermal transmission, which is suitable for use in medical applications. The rest of the paper is organized as follows: Section 2 discusses related literature. Section 3 discusses the suggested system and channel model, while Section 4 derives a closed-form solution for the average SNR, the outage probability, the outage rate, and the average capacity. Numerical results are presented in Section 5, while the conclusion and future work are discussed in Section 6.

2 RELATED WORK

Over the past few decades, researchers worldwide have published numerous studies on optical transdermal transmission. Transdermal wireless connections have been studied and documented in various research projects. In vitro and in vivo experiments were conducted to demonstrate the superiority of optical wireless transmission over RF technology. In [5], a data rate of about 75 Mbps was achieved when conducting an in-vitro study on a 6 mm layer of pork skin, which has similar optical properties to human skin [6]. In [7], the same researchers used a 2.5 mm skin thickness of an anesthetized sheep in an in vivo experiment, achieving a bit error rate (BER) of less than $2x10^{-7}$ while consuming 2.1 mW and achieving speeds of up to 100 Mb/s. However, they did not account for any misalignment between the receiver terminals and the transmitter. In [8], a vertical-cavity surface-emitting laser diode (VCSEL) with an 850nm wavelength and an active area of 7 mm^2 and a PIN photodiode with a 2–8 mm thickness of pork tissue were implemented. The system employed Manchester encoding to examine the feasibility of a transdermal telemetry link with a minimum beam divergence angle of 2° as an initiative to reduce optical power losses. A hybrid transdermal system of RF and infrared for cortical recording applications was demonstrated in [9]. Various configurations of emitters and detectors were tested at different data rates to assess power efficiency. Up to 40 Mbits/second data rate could be achieved through a skin thickness of 5 mm when 120 mW or less power is dissipated. Reducing the skin thickness to 3 mm will increase the data rate. Less than 20 Mbits/s could be easily achieved using various components and optical technology. Receivers need to be aligned within 1–2 mm of the center in order to function. The scattering presents the primary challenge and limiting factor affecting performance in the application, especially in fatty tissues, with a typical optical recovery factor of 0.5% to 5% over a diffuse area.

In vivo experiments were conducted on the brains of rats and monkeys as part of an extensive study using a hybrid model [10]. Under anesthesia, implants were

placed inside the brain to record the somatosensory neural activity of a rat and the motor neural activity of a monkey. An external electronic unit received the signal for audio and video display and digitization. A model for bidirectional transdermal optical transmission using wavelength division and amplitude shift keying (ASK) was developed [11]. In reference [12], the authors examined two link configurations—direct links and retro—to illustrate the possibility of establishing a retro-reflective transcutaneous optical wireless link using chicken dermis. In a direct link, a light source inside the body transmits data to a receiver outside the body, crossing the skin only once. In the retro link configuration, the light beam is reflected back to its source by the in-body unit, modulated through the modulating retro-reflector (MRR), and then captured outside the body by the photodiode. Because most of the experiments were conducted on anesthetized animals, fixed numbers were used to represent the pointing errors in terms of BER. This approach has major disadvantages as it does not accommodate stochastic behavior.

The authors [13] studied the outage performance of TOW links, taking into account the limitations of PEs, channel characteristics, and the physical constraints associated with in-body devices. The authors mentioned that for a fixed normalized signal-to-noise ratio (SNR) value, the outage performance (measured by the outage probability) increases as the misalignment between the transmitting and receiving units becomes more severe. As the normalized SNR increases, the limitations of pointing errors (PEs) on the outage probability become more apparent. This study also illustrates the outage probability in relation to the wavelength for various threshold SNR values, denoted as γ_{th}. For a given operating wavelength with a minimum SNR value, i.e., the threshold value, the outage probability deteriorates. In this study, the authors concluded that wavelength values ranging from 400 to 600 nm and wavelengths around 1500 nm are unsuitable for TOW transmission, while values around 1100 nm are considered the optimal wavelength. The authors [14] studied the use of an optimal combining method at the receiver side of the TOW communication interface. The proposed design consists of out-of-body, in-body units, and skin. At the transmitting unit, this system design incorporates two modulation schemes: on-off keying (OOK) and pulse position modulation (PPM). Based on the assumption that the stochastic PE component in the total channel coefficient has an upper limit, the support of the probability density function (PDF) was considered. This led to the reflection of all the analytical work for the average BER and the expressions, resulting in the availability of generalized error performance results. The use of this combining method, combining receive diversity with PPM, significantly enhances error performance. [15], with the goal of assessing TOW performance, integrated the outage probability metric into the study conducted by [14] using the same channel conditions. [16] developed an OWC-based system model aimed at improving the reliability, spectral efficiency, and power efficiency of a transcutaneous link in a cochlear implant. The proposed model incorporates all the design parameters and their corresponding interactions, such as skin thickness, optic area size, misalignment severity for both the transmitter and receiver, system efficiency, and transmitted power. The closed-form expression derived in [16] provides the average SNR, OP, ergodic spectral efficiency, and the capacity of the link.

3 SYSTEM AND CHANNEL MODEL

Figure 1 illustrates the components of the transcutaneous communication model under consideration. Three main components are present: the internal (in-body) unit, the skin representing the channel, and the external (out-of-body) unit.

The TOW system model under study uses DPSK, which has been demonstrated to be effective in free-space optical wireless systems [18]. In this paper, we consider a transdermal transmission process where a stimulation message is emitted through the skin.

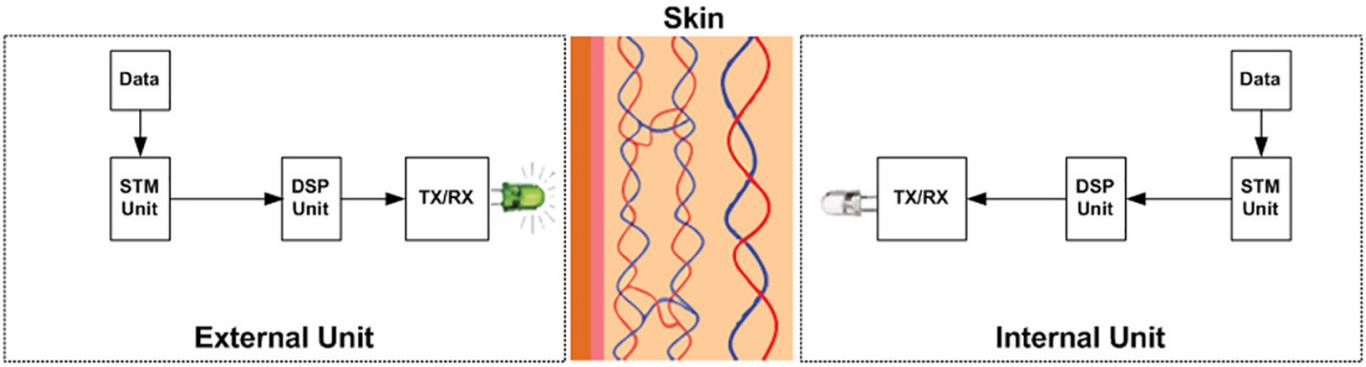

Fig. 1. TWO system model [17]

From the external unit to the internal unit. When the transmitted signal, x, passes through a channel, h, in the presence of noise n, the received signal of baseband equivalent can be defined as [15].

$$y = R.\,hx + n \tag{1}$$

In this equation, R represents the receiver's photodiode responsivity, which is used to measure the input and output gain for a detector system. It is expressed in units of amperes per watt (A/W) or volts per watt (V/W) and can be figured out via $R = \eta \frac{q}{pv}$, where, η represents the photodiode quantum efficiency, q represents the charge of the electron, v represents the frequency of the photons, and p represents the Planck constant [15].

On its journey from the transmitter to the receiver, the emitted light encounters two channel gain elements. The first element is deterministic and exclusively represents the propagation loss, specifically the skin attenuation. The second term refers to stochastic terminology and represents the geometric distribution caused by misalignment between the transmitter and receiver ends. The product of the two components yields the net channel coefficient, h [12, 19]:

$$h = h_l h_p \tag{2}$$

Where h_l is the deterministic component of the channel coefficient, and h_p denotes the stochastic component of the channel coefficient. h_l can be defined as shown in references [3, 13, 20]:

$$h_l = exp\left(-\frac{1}{2}\alpha(\lambda)\delta\right) \tag{3}$$

Where $\alpha(\lambda)$ represents the coefficient of skin attenuation at a given wavelength λ, and δ denotes the skin thickness.

The skin thickness, δ, determines the communication distance between the transmitter and the receiver unit. Due to the presence of skin attenuation in this channel, it is necessary to consider and measure $\alpha(\lambda)$, which represents the skin attenuation

coefficient at wavelength λ. The values of $\alpha(\lambda)$ depend on the skin's optical characteristics within the range of 400–1800 nm and can be expressed as [13, 14, 20]:

$$\alpha(\lambda)=\sum_{i=1}^{8} a_i \exp\left[-\left(\frac{\lambda-b_i}{c_i}\right)^2\right] \tag{4}$$

In [13], Table 1 presents the numerical values of a_i, b_i, and c_i for i = 1 through 8, and where λ is provided in nm.

The biggest challenge related to the reliability and performance of transcutaneous links is the misalignment between the transmitter aperture and the receiver. This misalignment is perceived as an offset occurring in the line between the beam footprint and the detector, as seen at the detector plane.

The only parameter considered in the current paper is the jitter component, i.e., the zero-boresight PE. It follows the same framework as seen in [20] to determine the stochastic expression, h_p, which represents the fraction of collected power resulting from the geometric spread with a radial displacement, r, from the central zone of the detector. This is approximately calculated by the Gaussian function as [3, 13, 16, 20]:

$$h_p \approx A_O \exp\left(-\frac{2r^2}{\omega_{eq}^2}\right) \tag{5}$$

Where A_o is the fraction related to the collected power with a radial offset of zero. A_o can be calculated by [3, 13, 16, 20]:

$$A_o = [ref(v)]^2 \tag{6}$$

Where $ref(v)$ is the error function related to the value v. The value v can be calculated using [3, 13, 16, 20]:

$$v = \frac{\sqrt{\pi}\,a}{\sqrt{2}\omega_\delta} \tag{7}$$

Here a denotes the receiving aperture radius, δ denotes the thickness of the skin, and ω_δ represents the waist of the beam at the RX plane. In addition, δ is measured by [3, 13, 16, 20]:

$$\omega_\delta = \delta \tan\left(\frac{\theta}{2}\right) \tag{8}$$

Here, θ represents the transmitted beam divergence angle. We therefore assumed that the skin layer is in direct contact with both the transmitter and the receiver. Practically, δ range from 4 to 10 mm [21]. In equation (5), the ω_{eq} value represents the radius of the equivalent beam, as defined in [3, 13, 16, 20]:

$$\omega_{eq}^2 = \omega_\delta^2 \frac{\sqrt{\pi}\ erf(v)}{2v\,exp(-v^2)} \tag{9}$$

The value of r, the radial displacement, in equation (5) is expressed as [22]:

$$r = \sqrt{r_x^2 + r_y^2} \tag{10}$$

Where r_x represents the displacement along the horizontal axis at the detector plane, and r_y represents the displacement along the vertical axis. These values are considered to be zero-mean Gaussian variables with equivalent and equal to σ_s^2 i.e., $r_x \sim N(0,\sigma_s^2)$, and $r_y \sim N(0,\sigma_s^2)$. Therefore, r follows a Rayleigh distribution, and PDF is expressed by [3, 13, 16, 20]:

$$f_r(r) = \frac{r}{\sigma_s^2} exp\left(-\frac{r^2}{2\sigma_s^2}\right) \quad r > 0 \tag{11}$$

The PDF of h_p, by using the appropriate transformation on (5) using the PDF in (11), is defined as [3, 13, 16, 20]:

$$f_{h_p}(x) = \frac{\xi}{A_0^{\xi}} x^{\xi-1},\ 0 \le x \le Ao \tag{12}$$

The severity of the PE, ξ, (where a lower value indicates a worse misalignment situation) can be expressed as [3, 13, 16, 20]:

$$\xi = \frac{\omega_{eq}^2}{4\sigma_s^2} \tag{13}$$

Values ranging from 0.1–2 of ξ correspond to the practical values [20]. Equation (13) shows that lower numerical values of ξ are associated with higher values of σ_s, which predispose to more intense PEs circumstances. The approximation in equation (5) is well-known in the literature and has been utilized in numerous previous research studies [3, 13, 16, 20]. In fact, this corresponds to the defined value of hp, especially if $\frac{\omega_\delta}{a} > 6$ is achieved, providing less than 10^3 as a normalized mean squared error (NMSE) shown in [23]. Once the linear random variable transformation Y = aX [24] has been applied, the expression of the PDF related to the channel state h in (2), considering h_l is deterministic, can be provided as:

$$f_h(h) = \frac{\xi}{A_0^{\xi} h_l^{\xi}} h^{\xi-1},\ \ 0 < h < A_0 h_l \tag{14}$$

4 PERFORMANCE METRICS

4.1 Average signal to noise ratio

At the receiver, the signal-to-noise ratio (SNR) defines the quality of the data and the data rate across the link. Two fundamental noise sources are known to affect the receiver: electrical noise and noise generated from light striking the photodiode. For To achieve low power transmission, it is important to reduce the noise from these sources. This is crucial because the need for more signal power will increase to compensate for the noise, especially when a specific SNR is needed. As a result, the level of noise seems to affect the link's ability to meet certain technical requirements. Inputs from various sources, such as. shot and thermal noise, contribute to the electrical noise. Shot noise, for example, is considered to be the result of the random behavior of photocurrent electron formation [25]. By assuming differential

phase shift keying (DPSK) modulation, the SNR can be obtained using the method described in reference [26].

$$\gamma = \frac{\eta_e A T_s h}{p.v} \tag{15}$$

Here, η_e represents the quantum efficiency of the detector, A is the effective area of the RX's photodiode, T_s is the DPSK symbol interval, h defines the channel and can be expressed as in (2), p is the Planck constant, and v is the photon frequency and can be expressed as in (7). The statistics for channel h, as represented by the mean value of h [26], are as follows:

$$E[h] = \frac{\xi}{\xi + 1} A_0 h_l \tag{16}$$

Based on (15) and (16), the average SNR:

$$\bar{\gamma} = \frac{\eta_e A T_s}{p.v} E[h] \tag{17}$$

$$\bar{\gamma} = \frac{\eta_e A T_s \xi A_0 h_l}{p.v\ (\xi + 1)} \tag{18}$$

4.2 The outage probability

The term "outage probability" refers to the probability of communication links and information rates entering an outage state, which happens when the information rate falls below the required threshold SNR value and fails to meet it. The value of the instantaneous SNR γ that falls below the predefined threshold value is denoted as $\gamma_{\min}$. The outage probability can be expressed as the cumulative distribution function (CDF) of h [13]:

$$P(\gamma_{th}) = P(\gamma \le \gamma_{th}) = \mathrm{F}_h(h) \tag{19}$$

By the substitution of equation (15) in equation (19):

$$P\left(h \le \frac{\gamma_{th} p.v}{\eta_e A T_s}\right) = F_h\left(\frac{\gamma_{th} p.v}{\eta_e A T_s}\right) \tag{20}$$

For the evaluation of $F_h(x)$ the following equation is used:

$$F_h(X) = \int_0^X f_h(h) dh \tag{21}$$

Also, by the substitution of equation (14) in equation (21):

$$F_h(h) = \begin{cases} \dfrac{1}{A_0^{\xi} h_l^{\xi}} x^{\xi}, & 0 \le h \le \mathrm{A}_0 \\ 1 \qquad , & h \ge A_0 \end{cases} \tag{22}$$

Finally, by using equations (20) and (22) the outage probability is:

$$P_{out} = \begin{cases} \left(\dfrac{\gamma_{th} p.v}{\eta_e A T_s A_0 h_l} \right)^{\xi} & 0 \le h \le A_0 \\ 1 & h \ge A_0 \end{cases} \tag{23}$$

4.3 The outage rate

The average rate at which service interruptions occur. The average outage rate is defined as [27]:

$$R_{out} = (1 - P_{out}) B Log_2 (1 + \gamma_{th}) \tag{24}$$

By the substitution of equation (23) in equation (24)

$$R_{out} = \begin{cases} \left(1 - \left(\dfrac{\gamma_{th} p.v}{\eta_e A T_s A_0 h_l} \right)^{\xi} \right) B Log_2 (1 + \gamma_{th}) , & 0 \le h \le A_0 \\ 0 , & h \ge A_0 \end{cases} \tag{25}$$

4.4 The average capacity

The channel capacity is defined as the maximum rate at which information can be reliably transmitted over the channel with a negligible probability of error. This performance evaluation is measured in bits per second (bps) per Hertz and is calculated using Shannon's Formula [27, 28]:

$$C = B Log_2 (1 + \gamma) \tag{26}$$

Where B is the signal bandwidth. To evaluate the average capacity, the estimation of equation (26) is utilized as:

$$\bar{C} = E\left[B Log_2 (1 + \gamma) \right] = E\left[B \frac{\ln[1 + \gamma]}{\ln(2)} \right] = \frac{B}{\ln(2)} E\left[\ln[1 + \gamma] \right] \tag{27}$$

$$\bar{C} = \frac{B}{\ln(2)} \int_0^K \ln[1 + \gamma] f_\gamma(\gamma) d\gamma \tag{28}$$

Where $(K = A_0 h_l)$, and $f_\gamma(\gamma)$ represents the PDF of γ.
$f_\gamma(\gamma)$ Expressed as:

$$f_\gamma(\gamma) = \frac{f_h(h)}{d\gamma / dh} , \quad \text{at } h = \frac{\gamma \ p.v}{\eta_e A T_s} \tag{29}$$

By the substitution of equation (14) in equation (29)

$$f_\gamma(\gamma) = \frac{\dfrac{\xi}{A_0^{\xi} h_l^{\xi}} h^{\xi - 1}}{\dfrac{\eta_e A T_s}{p.v}} \tag{30}$$

Then by substitution of $h=\frac{\gamma p.v}{\eta_e AT_s}$ in (30)

$$f_\gamma(\gamma)=\frac{\frac{\xi}{A_0^\xi h_l^\xi}\left(\frac{\gamma p.v}{\eta_e AT_s}\right)^{\xi-1}}{\frac{\eta_e AT_s}{p.v}}=\frac{\xi}{\gamma}\left(\frac{\gamma p.v}{A_0 h_l \eta_e AT_s}\right)^\xi \tag{31}$$

By using (31) in (28)

$$\bar{C}=\frac{B}{\ln(2)}\int_0^K \ln[1+\gamma]\xi\gamma^{\xi-1}\left(\frac{p.v}{A_0 h_l \eta_e AT_s}\right)^\xi d\gamma \tag{32}$$

By utilizing the equation (11) in [29] in equation (32) then

$$\bar{C}=\frac{B}{\ln(2)}\xi\left(\frac{pv}{A_0 h_l \eta_e AT_s}\right)^\xi \int_0^K \gamma^{\xi-1} G_{1,2}^{2,2}\left(\gamma\middle|\begin{matrix}1, & 1\\ 1, & 0\end{matrix}\right)d\gamma \tag{33}$$

When equation (26) in [29] is used, the final equation presents as:

$$\bar{C}=\frac{B}{\ln(2)}\xi\left(\frac{pv}{A_0 h_l \eta_e AT_s}\right)^\xi (A_0 h_l)^{\xi+1} G_{3,3}^{1,3}\left(A_0 h_l\middle|\begin{matrix}1, & 1, & -\xi\\ 1, & -(1+\xi), & 0\end{matrix}\right) \tag{34}$$

4.5 Numerical results

Transdermal optical wireless link parameters are utilized here to generate the results, as depicted in Table 1. Taking into consideration that the value of certain parameters is selected from references [3, 20, 30]. This paper evaluates the performance of the TOW link, assuming that the light source is a laser emitting DPSK pulses with an operating wavelength of 850 nm. It is also assumed that the pulses traverse a 4 mm thickness of the skin layer. A circular photodetector with a radius of 0.5 mm then collects the optical signal with a conversion ratio, or responsivity, of 0.7 A/W.

Figure 2 illustrates how the skin thickness impacts the quality of the received signal for the TOW link. Note, however, that both the analytical and simulation outcomes match. Therefore, the analytical context related to the average SNR derivation is verified. For a given wavelength, the average SNR decreases as the thickness of the skin increases, i.e., getting a degraded received signal as a result of path loss. Furthermore, it is observed that the average SNR depends on the wavelength for a given skin thickness, δ. As an example, if δ equals 6 mm and λ equals 1500 nm, then the average SNR will be 48 dB, while if δ remains the same and λ equals 1400 nm, the average SNR will increase to 75 dB, indicating a 25% improvement in the quality of the signal solely by decreasing the wavelength by 100 nm. However, on the other hand, changing the wavelength from 400 nm to 500 nm while keeping the same value of δ improves the average SNR by about 35%.

Table 1. The values of TOW link parameters

Parameters	Value
R (Receiver Responsivity)	0.7 A/W
θ (Beam divergence angle)	20°
P_s (Signal PSD)	1 mW/Hz
B (Signal Bandwidth)	10 MHz
λ (Signal Wavelength-Laser Source-)	850 nm
α(λ) (kin Attenuation Factor) for λ = 850 nm	1.8 nm
δ (Skin Thickness)	4 mm
α (Aperture Radius)	0.5 mm
σ (Pointing error)	1.4422 mm
A (The RX's Photodiode Effective Area)	1 mm^2
η_e (Quantum Efficiency)	0.8 A/w
Ts (DPSK Symbol Interval)	$1*10^{-9s}$

It is important to properly select the wavelength when designing a TOW link. In addition, it has been found that if δ is less than or equal to 5.5 mm, a link with 1500 nm outperforms a link that operates at 400 nm, whereas if it is more than 5.5 mm, the opposite is observed. Accordingly, if the skin thickness is 5.5 mm or less, the RX's responsivity is the main factor determining the degradation of the signal quality. However, when the thickness exceeds 5.5 mm, the dominant factor is the skin attenuation coefficient.

Figure 3 illustrates the impact of the wavelength on the average SNR for different values of the jitter standard deviation, σ. There was an increase in the average SNR. In addition, the average SNR decreases for a defined wavelength as σ increases. If λ is equal to 600 nm, there will be a 10% decrease in the average SNR when σ increases by 1 from 0.25 to 1.25. Furthermore, the figure also illustrates the presence of a transmission window within the wavelength range of 700 nm to 1300 nm. In this range of wavelengths, there are various commercial LEDs and several photodiodes available. The wavelength of around 1500 nm is found to be suboptimal for use in the TOW link, and a wavelength of 1100 nm is considered optimal.

Figure 4 illustrates the impact of the skin thickness, δ, on the quality of the received signal by displaying the effect of various values of the jitter SD, σ_s, on the average SNR. Here, the average SNR value decreases as both the skin thickness and the Jitter SD increase. As an example, if the skin thickness is 6 mm and the Jitter SD changes from 0.1 to 1 mm, a decrease in the average SNR value of less than 10% is noticed. The same principle applies when increasing the skin thickness for a specified Jitter SD. For example, if the Jitter SD is 0.5 mm and the skin thickness varies from 4 to 10 mm, a 30% decrease in the average SNR value is observed. Similarly, for the same skin thickness as before, if the Jitter SD is 1 mm, a decrease in the average SNR of about 20% is observed. In conclusion, when σ_s is increased, the impact of skin thickness on signal quality diminishes.

Figure 5 illustrates the impact of the effective area of the photodiode, A, on the average SNR for various jitter SD values, σ_s. As the figure demonstrates, for a specific value of σ_s, an increase in the PD effective area leads to a higher average SNR value.

As A values increase, the performance improvement becomes less significant. This clearly shows that, beyond a certain point, the impact of A on performance becomes insignificant. Moreover, for a specific A, when the jitter standard deviation SD, σ_s, increases, the signal quality degrades and the average SNR decreases. Additionally, for a given A, as the jitter SD, σ_s, increases, the signal quality deteriorates and the average SNR decreases.

Figure 6 illustrates how the wavelength's impact on the average SNR varies with the skin thickness, δ. A rise in the average SNR was observed, indicating that the TOW link is significantly more energy efficient than the RF link. In addition, the average SNR decreases for a defined wavelength as δ increases. The figure also illustrates the presence of a transmission window in the wavelength range of 700 nm to 1300 nm. In this range of wavelengths, a variety of commercial LEDs and several photodiodes are available. A wavelength of approximately1500 nm is found to be suboptimal for use in the TOW link, while a wavelength of 1100 nm is considered optimal.

In Figure 7, the graph illustrates the impact of wavelength on the outage probability for various SNR threshold values, γ_{th}, assuming a PEs severity of $\zeta = 1$ and using equation (23). For a given wavelength, as the SNR threshold rises, the outage probability will also increase, as expected. For example, if λ is equal to 650 nm, then increasing γ_{th} from 0.07 to 1 will result in a 10% increase in the outage probability.

Figure 8 illustrates the effect of skin thickness on the outage probability for various SNR threshold values when λ is equal to 1500 nm. We observed compatibility in the results, and thus, the analysis of outage probability was basically ascertained. Based on a fixed skin thickness, an increase in γ_{th} results in a higher outage probability. For instance, if δ is equal to 8 mm and γ_{th} is equal to 0.5, then the outage probability will be approximately $1.1*10^{-6}$. In the same way, for the same δ, if γ_{th} increases to 3, the outage probability will be approximately $1.4*10^{-6}$. In addition, given a fixed value of γ_{th}, if δ exceeds 8 mm, we observe an increase in the outage probability. The reason for this is that the transmission is severely affected by pointing errors when the Tx-Rx distance is close (skin thickness is less than or equal to 6 mm). In other words, an increase in skin thickness leads to a decrease in the effectiveness of the PEs, making the impact of path gain more pronounced.

Both equations (23) and (25) are utilized to calculate numerical results for outage probability and outage rate. By employing different SNR threshold values, Figure 9 illustrates the effect of PEs on the Outage Performance of the transdermal link. As shown in this figure, there are significant fading effects under acute pointing error conditions. In contrast, these deep fading situations get greater immunity with moderate pointing errors. For example, if the SNR_{th} value is 15 dB, and the responsivity (R) of the photodetector at the receiver is 0.7, then the Outage Probability will be approximately 10^{-4}. Figure 10 illustrates the impact of the wavelength, λ, on the outage rate for various SNR threshold values, γ_{th}. As the figure demonstrates, as the value of γ increases, there will be a decrease in the outage rate, and the signal quality improves. Figure 11 depicts the average capacity as a function of the wavelength for various PE values, by using equation (34). As indicated here, for a fixed wavelength, as the values of PE increase (transitioning from a weak to a severe state), the average capacity also increases. For instance, for λ is equal to 1500 nm and ζ is equal to 2, the average capacity is approximately 12. While for the same λ, when ζ becomes 1, the average capacity decreases to 8.

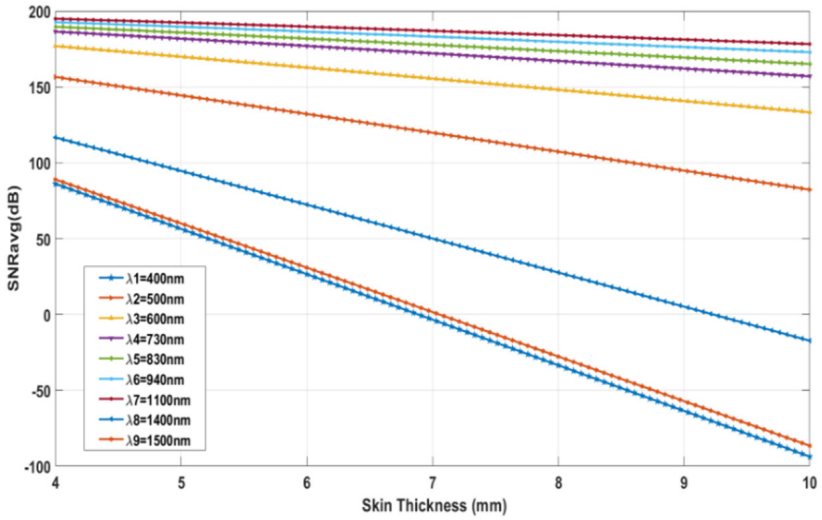

Fig. 2. Average SNR vs. skin thickness, under several wavelengths

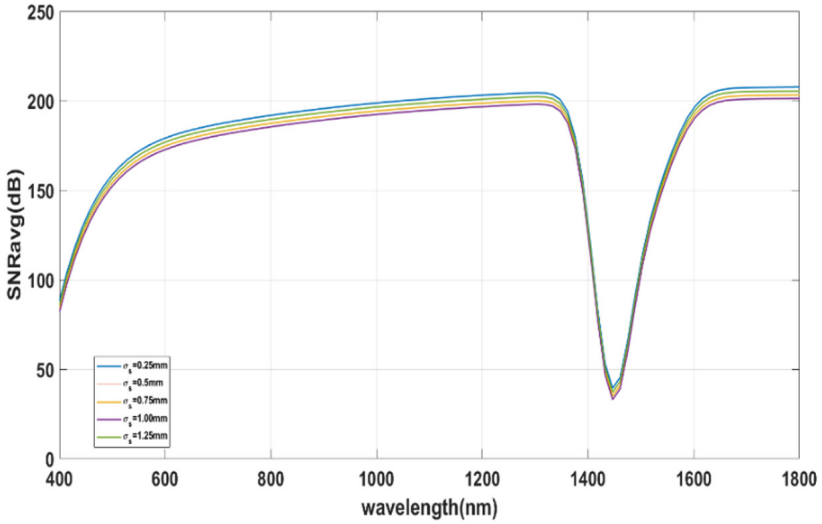

Fig. 3. Average SNR vs. wavength, λ under several values of σ_s

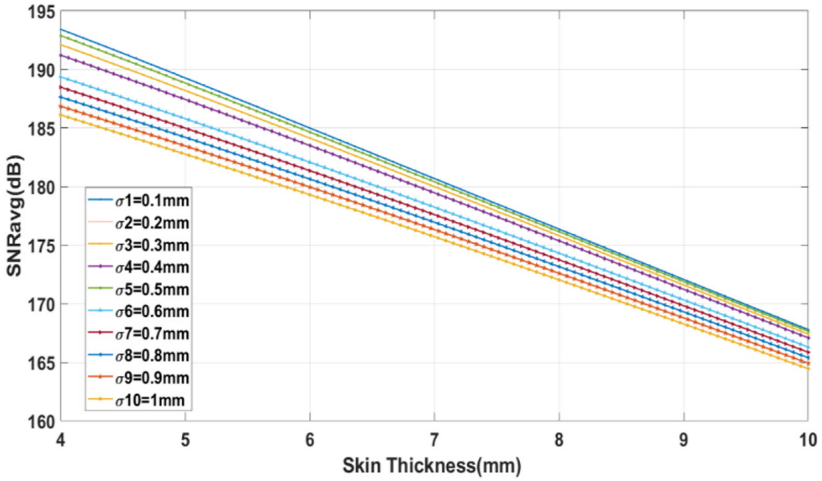

Fig. 4. Average SNR vs. skin thickness, δ under several values of σ_s

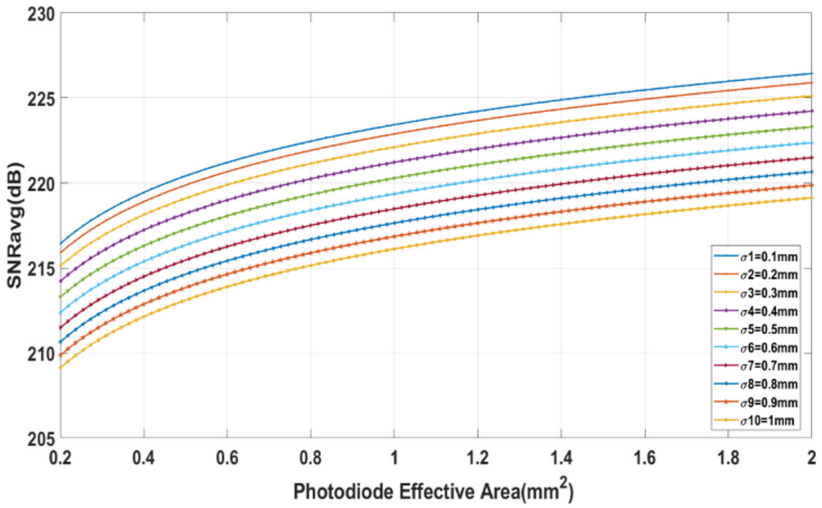

Fig. 5. Average SNR vs. photodiode effective area, A under several values, σ_s

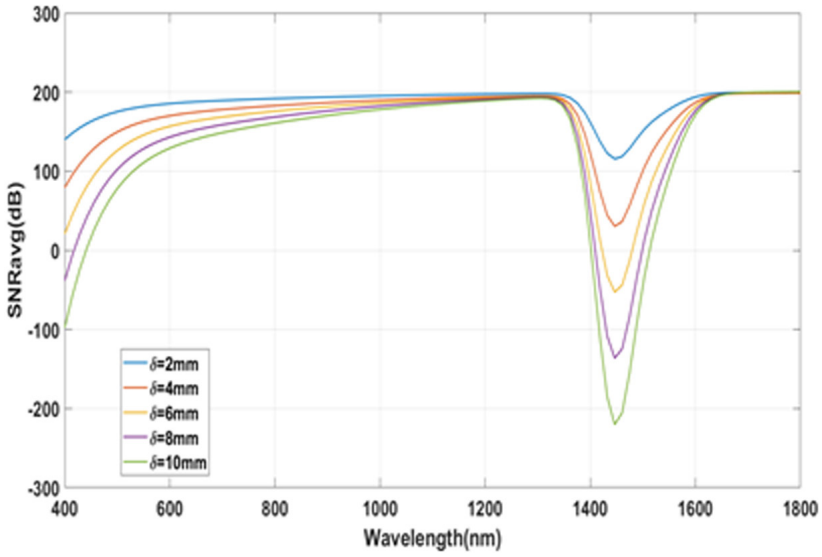

Fig. 6. Average SNR vs. wavelength, λ under several values of skin thickness, δ

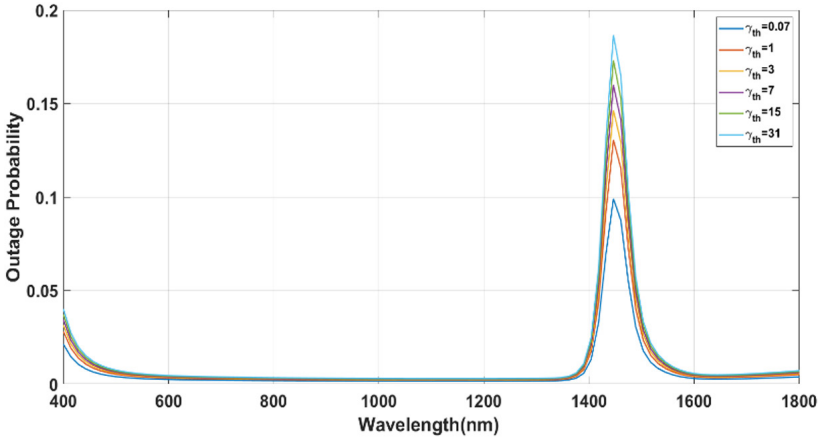

Fig. 7. Outage probability vs. wavelength, under several values of threshold SNR

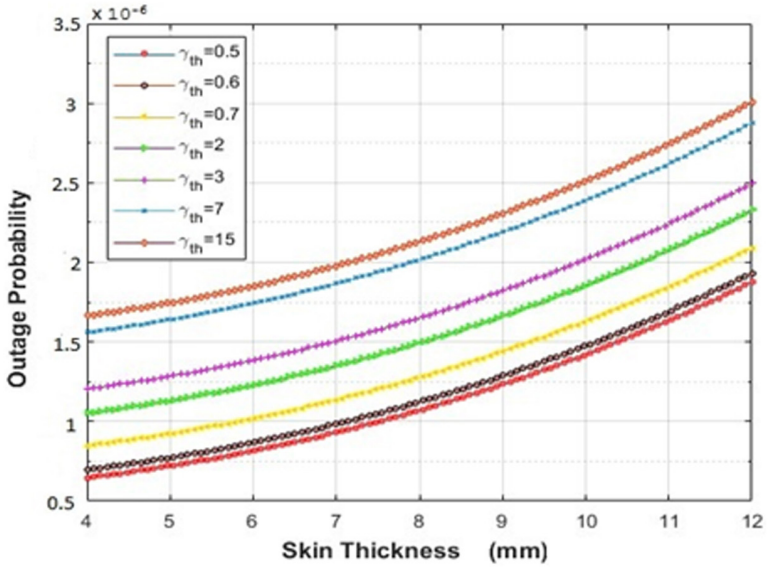

Fig. 8. Outage probability vs. skin thickness, under several values of threshold SNR

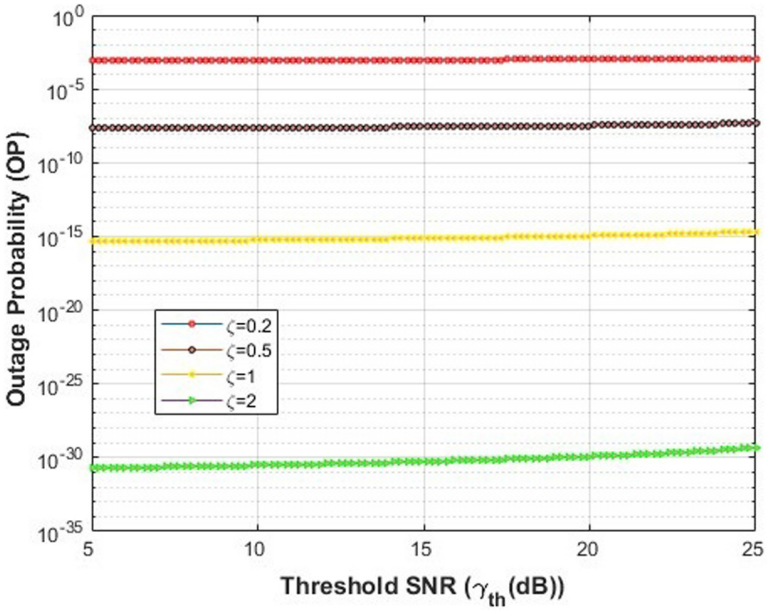

Fig. 9. Outage probability vs. threshold SNR under several values of PE severity

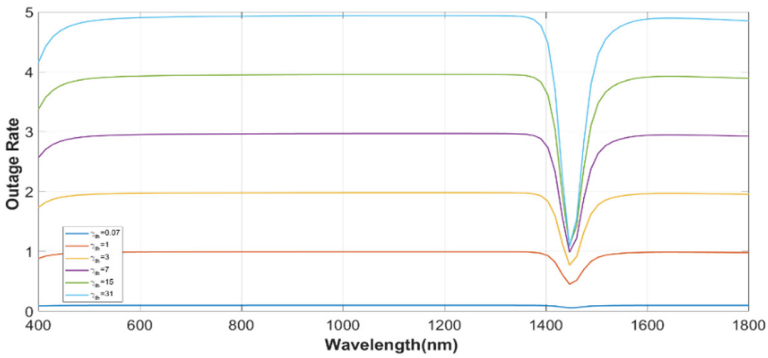

Fig. 10. Outage rate vs. wavelength under several values of threshold SNR

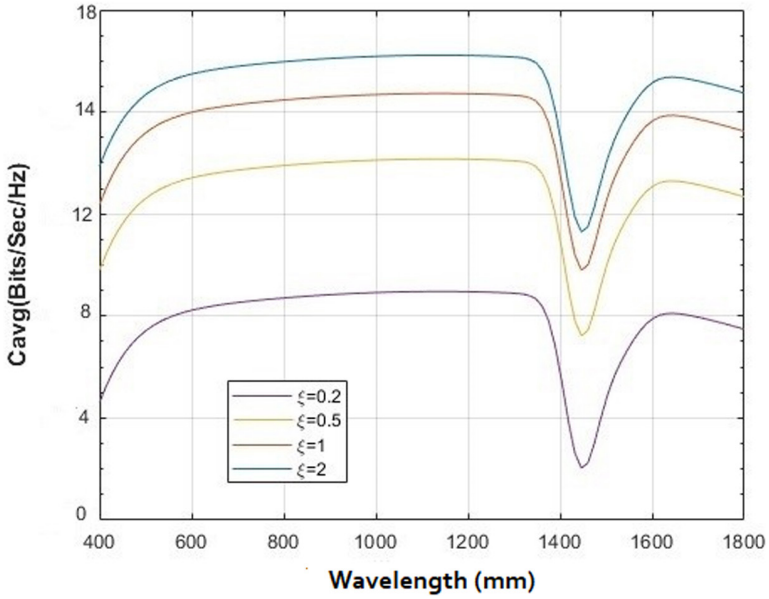

Fig. 11. Average capacity vs. wavelength under several values of PE severity

5 CONCLUSION

According to the results obtained, the most crucial factor affecting the quality and effectiveness of the TOW link was the absence of boresight pointing errors. The impact of PE is shown to have a detrimental effect on the performance of the TOW link. In this study, we utilized DPSK modulation to examine its impact on overall performance. The achieved average SNR, outage probability, outage rate, and average capacity results demonstrate a significant improvement over OOK modulation, with a calculated 3 dB higher performance. A better performance is reported for the average outage rate, as expected when using DPSK modulation. The seriousness of pointing errors significantly impacts the outage rate. A transmission wavelength window for TOW applications exists within the range of 700–1300 nm. In addition, the optimal transmission wavelength is 1100 nm.

6 REFERENCES

[1] G. Elamare, "Investigation of high bandwith biodevices for transcutaneous wireless telemetry," PhD diss., Newcastle University, 2010. https://theses.ncl.ac.uk/jspui/bitstream/10443/994/1/Elamare10.pdf

[2] J. L. Abita and W. Schneider, "Transdermal optical communications," *Johns Hopkins Apl. Technical Digest*, vol. 25, no. 3, pp. 261–68, 2004. https://www.jhuapl.edu/techdigest/TD/td2503/Abita.pdf

[3] Trevlakis, E. Stylianos, Alexandros-Apostolos A. Boulogeorgos, and George K. Karagiannidis, "Signal quality assessment for transdermal optical wireless communications under pointing errors," *Technologies*, vol. 6, no. 4, p. 109, 2018. https://doi.org/10.3390/technologies6040109

[4] Alexandros-Apostolos A. Boulogeorgos, Stylianos E. Trevlakis, and Nestor D. Chatzidiamantis, "Optical wireless communications for in-body and transdermal biomedical applications," *IEEE Communications Magazine,* vol. 59, no. 1, pp. 119–125, 2021. https://doi.org/10.1109/MCOM.001.2000280

[5] Liu, Tianyi, Ulrich Bihr, Jens Anders, and Maurits Ortmanns, "Performance evaluation of a low power optical wireless link for biomedical data transfer," in *2014 IEEE International Symposium on Circuits and Systems (ISCAS)*, 2014, pp. 870–873. https://doi.org/10.1109/ISCAS.2014.6865274

[6] Cheong, Wai-Fung, Scott A. Prahl, and Ashley J. Welch, "A review of the optical properties of biological tissues," *IEEE Journal of Quantum Electronics*, vol. 26, no. 12, pp. 2166–2185, 1990. https://doi.org/10.1109/3.64354

[7] Liu, Tianyi, Ulrich Bihr, Joachim Becker, Jens Anders, and Maurits Ortmanns, "In vivo verification of a 100 Mbps transcutaneous optical telemetric link," in *2014 IEEE Biomedical Circuits and Systems Conference (BioCAS) Proceedings*, 2014, pp. 580–583. https://doi.org/10.1109/BioCAS.2014.6981792

[8] Parmentier, Stefan, Rejean Fontaine, and Yves Roy, "Laser diode used in 16 Mb/s, 10 mW optical transcutaneous telemetry system," in *2008 IEEE Biomedical Circuits and Systems Conference*, 2008, pp. 377–380. https://doi.org/10.1109/BIOCAS.2008.4696953

[9] K. S. Guillory, A. K. Misener, and A. Pungor, "Hybrid RF/IR transcutaneous telemetry for power and high-bandwidth data," in *The 26th Annual International Conference of the IEEE Engineering in Medicine and Biology Society*, 2004, vol. 2, pp. 4338–4340. https://doi.org/10.1109/IEMBS.2004.1404207

[10] Song, Yoon-Kyu, William R. Patterson, Christopher W. Bull, David A. Borton, Yanqiu Li, Arto V. Nurmikko, John D. Simeral, and John P. Donoghue, "A brain implantable microsystem with hybrid RF/IR telemetry for advanced neuroengineering applications," in *2007 29th Annual International Conference of the IEEE Engineering in Medicine and Biology Society*, 2007, pp. 445–448. https://doi.org/10.1109/IEMBS.2007.4352319

[11] Okamoto, Eiji, Yoshiro Yamamoto, Yusuke Inoue, Tsutomu Makino, and Yoshinori Mitamura, "Development of a bidirectional transcutaneous optical data transmission system for artificial hearts allowing long-distance data communication with low electric power consumption," *Journal of Artificial Organs*, vol. 8, pp. 149–153, 2005. https://doi.org/10.1007/s10047-005-0299-7

[12] Gil, Yotam, Nadav Rotter, and Shlomi Arnon, "Feasibility of retroreflective transdermal optical wireless communication," *Applied Optics*, vol. 51, no. 18, pp. 4232–4239, 2012. https://doi.org/10.1364/AO.51.004232

[13] Trevlakis, E. Stylianos, A. Alexandros-Apostolos, Boulogeorgos, and George K. Karagiannidis, "Outage performance of transdermal optical wireless links in the presence of pointing errors," in *2018 IEEE 19th International Workshop on Signal Processing Advances in Wireless Communications (SPAWC)*, 2018, pp. 1–5. https://doi.org/10.1109/SPAWC.2018.8445766

[14] George K. Varotsos, Hector E. Nistazakis, Konstantinos Aidinis, Fadi Jaber, and K. K. Mujeeb Rahman, "Transdermal optical wireless links with multiple receivers in the presence of skin-induced attenuation and pointing errors," *Computation,* vol. 7, no. 3, p. 33, 2019. https://doi.org/10.3390/computation7030033

[15] George K. Varotsos, Hector E. Nistazakis, George S. Tombras, Konstantinos Aidinis, Fadi Jaber, and K. K. Mujeeb Rahman, "On the use of diversity in transdermal optical wireless links with nonzero boresight pointing errors for outage performance estimation," in *2019 8th International Conference on Modern Circuits and Systems Technologies (MOCAST)*, 2019, pp. 1–4. https://doi.org/10.1109/MOCAST.2019.8741807

[16] Stylianos E. Trevlakis, Alexandros-Apostolos A. Boulogeorgos, Paschalis C. Sofotasios, Sami Muhaidat, and George K. Karagiannidis, "Optical wireless cochlear implants," *Biomedical Optics Express*, vol. 10, no. 2, pp. 707–730, 2019. https://doi.org/10.1364/BOE.10.000707

[17] Stylianos E. Trevlakis, Alexandros-Apostolos A. Boulogeorgos, and George K. Karagiannidis, "Outage performance of transdermal optical wireless links in the presence of pointing errors," in *2018 IEEE 19th International Workshop on Signal Processing Advances in Wireless Communications (SPAWC)*, 2018, pp. 1–5. https://doi.org/10.1109/SPAWC.2018.8445766

[18] Huang, Xinning, Xiaoping Xie, Jiazheng Song, Tao Duan, Hui Hu, Xin Xu, and Yulong Su, "Performance comparison of all-optical amplify-and-forward relaying FSO communication systems with OOK and DPSK modulations," *IEEE Photonics Journal*, vol. 10, no. 4, pp. 1–11, 2018. https://doi.org/10.1109/JPHOT.2018.2852301

[19] Liu, Tianyi, Jens Anders, and Maurits Ortmanns, "System level model for transcutaneous optical telemetric link," in *2013 IEEE International Symposium on Circuits and Systems (ISCAS)*, 2013, pp. 865–868. https://doi.org/10.1109/ISCAS.2013.6571984

[20] Stylianos E. Trevlakis, Alexandros-Apostolos A. Boulogeorgos, and George K. Karagiannidis, "On the impact of misalignment fading in transdermal optical wireless communications," in *2018 7th International Conference on Modern Circuits and Systems Technologies (MOCAST)*, 2018, pp. 1–4. https://doi.org/10.1109/MOCAST.2018.8376613

[21] Alexey N. Bashkatov, Elina A. Genina, and Valery V. Tuchin, "Optical properties of skin, subcutaneous, and muscle tissues: A review," *Journal of Innovative Optical Health Sciences*, vol. 4, no. 1, pp. 9–38, 2011. https://doi.org/10.1142/S1793545811001319

[22] Zhu, Bingcheng, Zhaoquan Zeng, and Julian Cheng, "Arbitrarily tight bounds on cumulative distribution function of Beckmann distribution," in *2017 International Conference on Computing, Networking and Communications (ICNC)*, IEEE, 2017, pp. 41–45. https://doi.org/10.1109/ICCNC.2017.7876099

[23] Ahmed A. Farid, A. Ahmed, and Steve Hranilovic, "Outage capacity optimization for free-space optical links with pointing errors," *Journal of Lightwave Technology*, vol. 25, no. 7, pp. 1702–1710, 2007. https://doi.org/10.1109/JLT.2007.899174

[24] Papoulis, Athanasios, and S. Unnikrishna Pillai, *Probability, Random Variables and Stochastic Processes*, 2002.

[25] Ackermann JR and Douglas Michael, *High Speed Transcutaneous Optical Telemetry Link*, PhD Thesis, Case Western Reserve University, 2008.

[26] Harilaos G. Sandalidis, T. A. Tsiftsis, and George K. Karagiannidis, "Optical wireless communications with heterodyne detection over turbulence channels with pointing errors," *Journal of Lightwave Technology*, vol. 27, no. 20, pp. 4440–4445, 2009. https://doi.org/10.1109/JLT.2009.2024169

[27] Omar Hasan, "Performance of heterodyne differential phase-shift keying system over double Weibull free-space optical channel," *Journal of Modern Optics*, vol. 62, no. 11, pp. 869–876, 2015. https://doi.org/10.1080/09500340.2015.1027311

[28] Omar Hasan, "Average capacity evaluation performance for transdermal optical wireless communications under the effect of pointing error," *International Journal of Online and Biomedical Engineering*, vol. 18, no. 13, pp. 84–96, 2022. https://doi.org/10.3991/ijoe.v18i13.33653

[29] Victor Adamchik and O. I. Marichev, "The algorithm for calculating integrals of hypergeometric type functions and its realization in REDUCE system," in *Proceedings of the International Symposium on Symbolic and Algebraic Computation*, 1990, pp. 212–224. https://doi.org/10.1145/96877.96930

[30] George K. Varotsos, Hector E. Nistazakis, Konstantinos Aidinis, Fadi Jaber, Mohd Nasor, and K. K. Mujeeb Rahman, "Error performance estimation of modulated retroreflective transdermal optical wireless links with diversity under generalized pointing errors," *Telecom*, vol. 2, no. 2, pp. 167–80, 2021. https://doi.org/10.3390/telecom2020011

7 AUTHORS

Yazeed Suleiman Al-Rbeihat received his MSc degree in Electrical Engineering, Princess Sumaya University for Technology (PSUT) in 2022, and BSc degree in Electrical Engineering from Hashemite University, in 2008. He is an expert in optical wireless communications and security systems as well as a certified trainer in many technologies, and is currently with Jordanian Public Security Directorate (PSD) (E-mail: yaz20208013@std.psut.edu.jo).

Prof. Omar M. Hasan (Bani Ahmad) received his PhD and MSc degrees in Communication Engineering, and BSc degree in Electrical Engineering from New Mexico State University, USA, 1996, 1990 and 1987 respectively. He joined Princess Sumaya University for Technology (PSUT) in 1997, where he chaired the communications engineering department at PSUT during the period 2005–2010. He has worked in the area of turbo coding and optical wireless communications, and has worked in different projects at physical science laboratory, Las Cruces, USA, 1991–1992 (E-mail: ohasan@psut.edu.jo).